Acta Cryst. (1959). **12**, 787

A Study of Pendellösung Fringes in X-ray Diffraction

By N. Kato and A. R. Lang

Division of Engineering and Applied Physics, Harvard University, Cambridge 38, *Massachusetts, U.S.A.*

(*Received* 26 *November* 1958)

X-ray topographs of a new type have revealed fine fringes in the diffraction images of wedge-shaped parts of perfect and nearly perfect crystals. The fringes are analogous to those seen in electron microscope images of wedge-shaped parts of magnesium oxide crystals and can be interpreted according to the theory applicable to the electron case. Fringe spacing depends upon X-ray wavelength, wedge-angle, inclination of reflecting plane to the wedge surfaces, and the structure amplitude of the reflection. Discovery of these fringes shows that (*a*) parts of real crystals behave as ideally perfect from the X-ray diffraction standpoint (*b*) the dynamical theory of diffraction may be applied quantitatively under practical experimental conditions, and (*c*) structure amplitudes of low-order reflections may be determined by fringe-spacing measurements, without any need for measuring reflection intensities. Tests of the theory on prepared wedges of silicon and quartz indicate a slight systematic discrepancy of 4 to 5% between calculated and observed values of structure amplitude, and suggest also that Wei's (1935) F-values for quartz $10\bar{1}\bar{1}$ and $\bar{1}\bar{1}22$ are too low by 9% and 4% respectively. Experiments suggest that to explain fully the observations some modification of the dynamical theory is required in the direction of allowing for a spherical wavefront of the incident beam.

1. Introduction

One of the authors (A. R. Lang) has constructed an X-ray spectrometer of a new type which can be operated automatically, and, using this apparatus, has established new techniques of diffraction microradiography which enable us to see individual dislocations in crystals (Lang, 1958, 1959). During these experiments we found very fine fringes in the diffraction topographs of wedge-shaped parts of a silicon crystal. These fringes are quite similar to those which were observed in electron microscope images of magnesium oxide by Heidenreich (1942), Kinder (1943) and Hall (1948). We call them 'Pendellösung' fringes because they are due to an intensity variation of wave field in the crystal which was called the 'Pendellösung' effect by Ewald (1916).

In this paper we show various examples of such fringes in lithium fluoride, silicon and quartz, and interpret them according to a theory which was developed for the electron case. Measurements of fringe spacings combined with this theory give us a very promising method for determining the structure amplitude of X-ray reflections without any measurement of X-ray intensities.

Our experiments indicate, however, that 'Pendellösung' fringes in the X-ray case are somewhat different from those in the electron case from the standpoint of diffraction phenomena. In the X-ray case the wave propagation behavior in the crystal is more complicated. In this paper we present only experimental facts and a very preliminary approach towards an extended theory. Still, we have concluded that we must modify the usual treatment of boundary conditions in the dynamical theory of diffraction, and must also consider the incident X-ray beam as a spherical wave.

2. Experimental

(i) *Apparatus*

We have used two types of apparatus. The first, which we call A, is the same as that used in studies of individual dislocations by transmission-type X-ray topographs called 'projection topographs' (Lang, 1959). The principle of this method is illustrated in Fig. 1. The X-ray beam is collimated by a slit system,

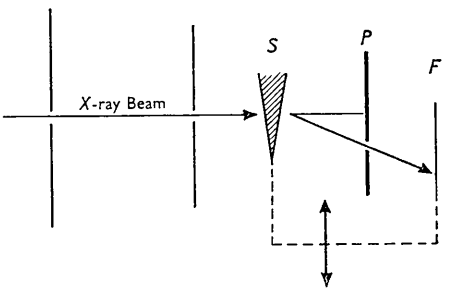

Fig. 1. Experimental arrangement for traverse experiments.

S is the specimen crystal and P is a slit through which only the diffracted beam is allowed to pass to reach the recording film F. Specimen and film are moved back and forth together. Thus we can record on the same film a diffraction topograph from a large area of crystal. We refer to this type of experiment as a 'traverse experiment', and to the pattern so obtained as a 'traverse pattern'.

With specimen and film stationary we obtain another type of pattern to which section parts of a crystal contribute as shown in Fig. 2. We call this type of experiment a 'section pattern'. In the present work we are interested in very fine details of section patterns and sometimes we have studied the corresponding section patterns due to the transmitted beam. For

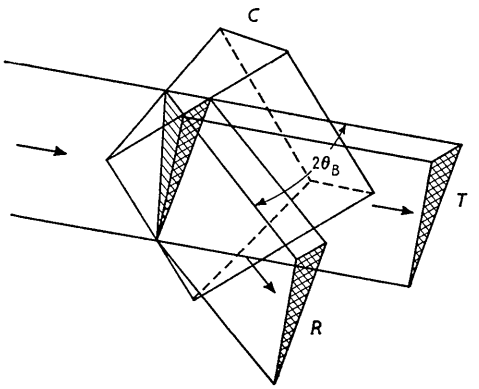

Fig. 2. Experimental arrangement for section experiments.

these purposes we use another apparatus which we call *B*. An incident beam of convergent monochromatized X-rays was produced by a transmission-type bent quartz monochromator. The geometrical arrangement of X-ray tube and monochromator was almost identical to that used in previous experiments on lattice distortions.* (Kato, 1957, 1958*a*). The focused breadth of the $K\alpha_1$ line was about 20μ and the $K\alpha_2$ was eliminated by a screen. To apparatus *B* there was also attached a device for moving the film and crystal automatically, as in apparatus *A*. Hence we could obtain similar traverse patterns, but with a monochromatized incident beam.

(ii) *Preparation of wedge-shaped crystals*

Preliminary traverse experiments were carried out to check crystal perfection, in particular the dislocation distribution. From dislocation-free parts of crystals wedge-shaped specimens were made by grinding. After that the crystals were etched to remove disturbed surface layers. For this purpose CP-4 and 48% HF solution were used for silicon and quartz respectively. Wedge angles were measured by an optical method.

(iii) *Traverse experiments*

We have obtained many 'Pendellösung' fringe patterns corresponding to various reflection planes of various crystals. Fig. 3 shows the first one that was obtained from a wedge-shaped part of a silicon single crystal, using the 111 reflection. In this case the wedge angle is about 40°. Fig. 4 is an example of fringes from a prepared regular wedge of silicon, the wedge angle being 21° 20′. This type of pattern was used for quantitative studies to be described in § 4. Fig. 5 is a projection topograph of part of a good-quality LiF crystal, taken with the 200 reflection. Many dislocations can be seen, but along the sub-grain boundaries 'Pendellösung' fringes can also be distinguished. Fig. 6 is an example of fringes from a prepared wedge of quartz. The main fringes are parallel to the edge of the wedge. We can also see areas of higher intensity in which there are additional fine fringes. The intensity of these areas depends upon the particular net plane from which reflection is observed. It appears that they represent plane defects, each of which divides the crystal into two wedge-shaped parts along which 'Pendellösung' fringes are produced.

Photographs were obtained by Ag $K\alpha_1$ radiation using apparatus *A* and by Mo $K\alpha_1$ radiation using apparatus *B*. Experimental details are given in the legend of each photograph.

(iv) *Section experiments*

As explained above in (i), we obtained section patterns using a fine monochromatized beam. Fig. 7 is an example of such a pattern: it is a 440 reflection from a silicon crystal. Image *a* is due to the diffracted beam and image *b* is due to the primary beam. In these patterns we see very interesting hook-shaped fringes. Light fringes in *a* correspond to dark fringes in *b*, and vice versa. This is an example of the complementarity of structure between diffracted and primary transmitted beams which we have generally observed, and which is particularly striking in the images of individual dislocations obtained in section experiments.

Similar patterns to Fig. 7 have been recorded on films placed far from the specimen.

3. Theory

The usual kinematic theory cannot be applied to the case of diffraction by large single crystals. For such problems the dynamical theory of diffraction in a three-dimensional lattice has been developed (see, for example, Zachariasen, 1945). In this theory we take into consideration the energy exchange between diffracted and transmitted waves when a phase relationship is maintained between them. It is thus found that, in passage through the crystal, the wave field of the primary beam at first decreases due to transfer of energy to the reflected beam, then energy is transferred back to the primary beam from the reflected beam, and so on. Hence the wave fields of both beams oscillate with a definite spatial periodicity within the crystal. Such an intensity modulation can be regarded as a sort of beat between plane waves. Actually, a more mathematical treatment shows that each wave field can be expressed as the interference of two plane waves which have slightly different wave vectors.

If the crystal is parallel plane-sided, as in the usual dynamical-theory treatment, these two plane waves come out of the crystal with the same wave vector. Therefore the wave field is uniform outside the crystal. However, if the crystal has a wedge-shaped form the

* In the present experiments a line source of X-rays is put parallel to the direction of the incident beam, because it is not necessary to have a wide angular range of convergence, but very desirable to get high intensity.

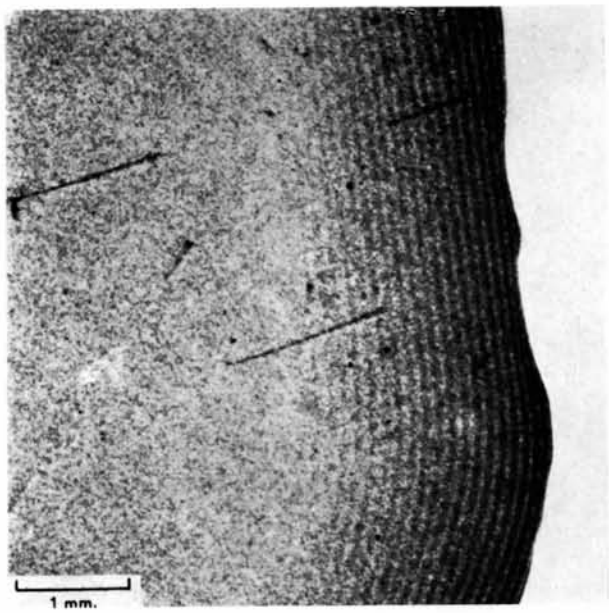

Fig. 3. Silicon 'Pendellösung' fringes: 111 reflection.

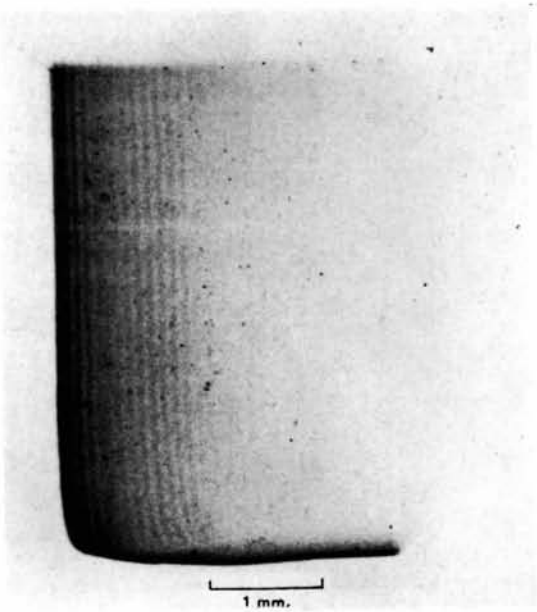

Fig. 4. An example of silicon {311} series of experiments. The wedge angle is 21° 20′. The edge direction is $[1\bar{1}0]$. The incident surface is (111). The reflecting net plane is $(3\bar{1}1)$. Configuration corresponds to Case I of Fig. 8.

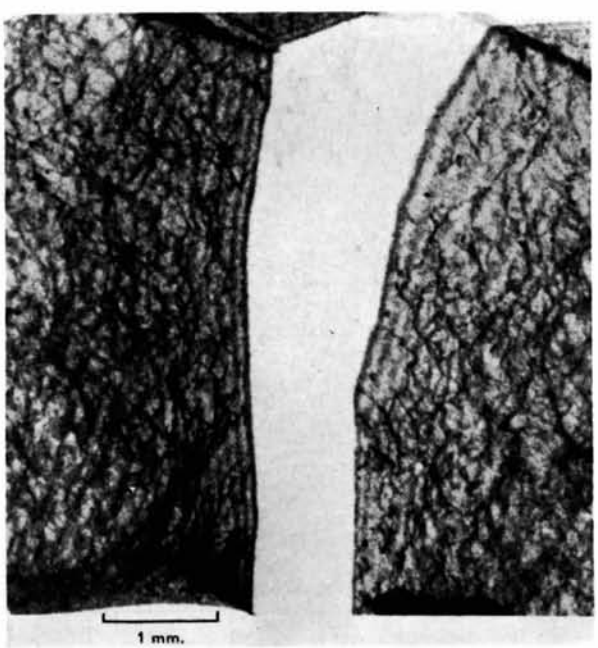

Fig. 5. Lithium fluoride 200 reflection.

(*To face p.* 788

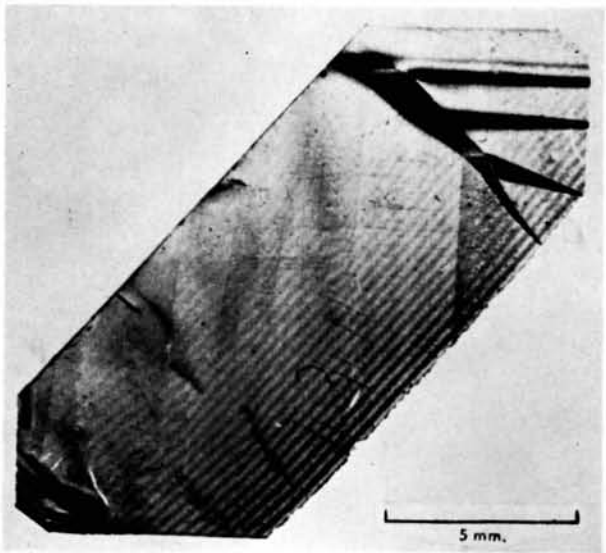

Fig. 6. An example of quartz R–r series. The wedge angle is 11° 16′, wedge direction is the Y-axis of quartz. The incident surface is the X-plane. The reflecting net plane is $(10\bar{1}1)$. Configuration corresponds to Case I of Fig. 9.

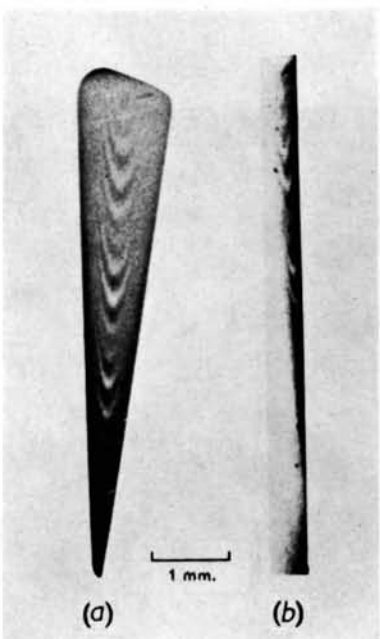

Fig. 7. Section patterns of silicon 440 reflection, (*a*) diffracted-beam pattern, (*b*) primary-beam pattern.

above two plane waves in the crystal emerge with different wave vectors, in a way analogous to double refraction in the optics of visible rays. This was pointed out first by M. v. Laue (1940), and later by Sturkey (1948) and Kato (1949) independently. Interference fringes may thus be expected outside the crystal. Actually, two Laue spots corresponding to the two plane waves described above can be observed in the electron diffraction case (Cowley & Rees, 1946, 1947; Honjo, 1953, Honjo & Mihama, 1954), and the interference fringes have been observed in electron microscope images as described in § 1. The explanation of these fringes was given by Kossel (1943) in principle and later by Kato (1953) and Niehrs (1954) in more detail.

The patterns we have obtained with X-rays are similar to those obtained with electrons, though the experimental conditions are very different. Since the angular range of reflection of the X-rays is very small, the crystal and film must be moved simultaneously to obtain this kind of pattern from an extended area of specimen when a narrow X-ray source is used. On the other hand, the electron microscope images are obtained by a single illumination from a point source. This is not a superficial difference in geometrical arrangement but is quite essential from the diffraction standpoint. More will be said about this in § 5. Nevertheless it is of considerable interest to compare the experimental results of the X-ray case with a theory which was developed for the electron case.

According to the dynamical theory for a large wedge-shaped crystal (Kato, 1949), the wave vectors of the two plane waves outside the crystal are

$$\begin{aligned}\mathbf{K}_g^{(1)} &= \mathbf{K}_0+2\pi\mathbf{g}+A_0\{(y-(y^2+1)^{\frac{1}{2}})\boldsymbol{\nu}_e/\cos\theta_G \\ &\quad +(y+(y^2+1)^{\frac{1}{2}})\boldsymbol{\nu}_a/\cos\varphi_G\} \\ \mathbf{K}_g^{(2)} &= \mathbf{K}_0+2\pi\mathbf{g}+A_0\{(y+(y^2+1)^{\frac{1}{2}})\boldsymbol{\nu}_e/\cos\theta_G \\ &\quad +(y-(y^2+1)^{\frac{1}{2}})\boldsymbol{\nu}_a/\cos\varphi_G\}\end{aligned} \tag{1}$$

where

$$A_0=\pi k_0 K|\psi_H'|\,(\cos\theta_G/\cos\theta_0)^{\frac{1}{2}}\,. \tag{2}$$

The notation in equations (1) and (2) is almost the same as that used by Zachariasen (1945). ψ_H' is a Hth order Fourier coefficient of the polarizability, that means, it is proportional to a structure factor. y is a parameter which shows an angular deviation of the incident beam from the Bragg angle. In addition, $\boldsymbol{\nu}_e$ and $\boldsymbol{\nu}_a$ are respectively unit vectors normal to the incident and exit surfaces, θ_G is the angle between $\boldsymbol{\nu}_e$ and the diffracted beam and φ_G is the angle between $\boldsymbol{\nu}_a$ and the diffracted beam. In these expressions we have neglected the mean polarizability of the crystal (or zero-th order component of the Fourier series representation of the polarizability), because this has no appreciable effect on the interference fringes. These formulae are derived directly from the electron case by appropriate changes of the quantities concerned.

The difference $\Delta\mathbf{K}$ of the two wave vectors is always approximately normal to the wave vectors $\mathbf{K}_g^{(1)}$ and $\mathbf{K}_g^{(2)}$ since their magnitude should be equal to $|K_0|$, the magnitude of the wave vector of the incident beam. Therefore, as we trace the interference pattern away from the crystal, the fringes move along parallel to the direction of the wave vectors $\mathbf{K}_g^{(1)}$ and $\mathbf{K}_g^{(2)}$. Hence, if we put a recording film perpendicular to the reflected beam, fringe spacings are given by

$$\begin{aligned}\Lambda &= 2\pi/|\Delta\mathbf{K}| \\ &= \lambda/\{K|\psi_H'|((1+y^2)\cos\theta_G/\cos\theta_0)^{\frac{1}{2}}\Phi\}\,.\end{aligned} \tag{3}$$

In equation (3) Φ is a geometric factor which can be written as

$$\begin{aligned}\Phi &= \left|\frac{\boldsymbol{\nu}_e}{\cos\theta_G}-\frac{\boldsymbol{\nu}_a}{\cos\varphi_G}\right| \\ &= \left\{\frac{1}{\cos^2\theta_G}+\frac{1}{\cos^2\varphi_G}-\frac{2\cos(\boldsymbol{\nu}_e\boldsymbol{\nu}_a)}{\cos\theta_G\cos\varphi_G}\right\}^{\frac{1}{2}}\end{aligned} \tag{4}$$

where $(\boldsymbol{\nu}_e\boldsymbol{\nu}_a)$ is the wedge angle.

$\Delta\mathbf{K}$ is also always perpendicular to the edge of the wedge, since $\Delta\mathbf{K}$ is in a plane determined by $\boldsymbol{\nu}_e$ and $\boldsymbol{\nu}_a$ and obviously the edge is perpendicular to this plane. This is what we observe experimentally, since the fringes always run parallel to the edge of the wedge.

Thus we see that fringe spacings can be calculated theoretically from well-known quantities such as the fundamental physical constants included in the expression $|\psi_H'|$, the X-ray wavelength, the structure amplitude, and geometrical quantities except for an unknown parameter y. For the present we assume that y is equal to zero, and will consider this point further in § 5.

For a comparison of the above theory with our experiments we have to introduce some formulae relating

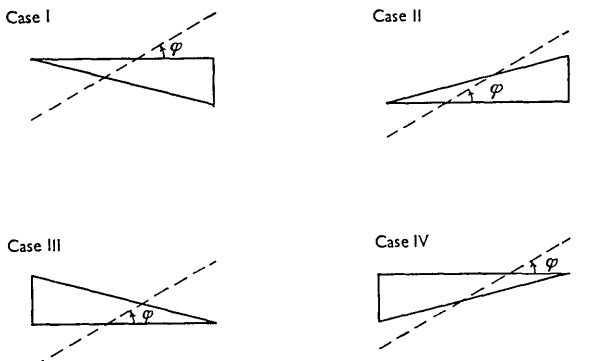

Fig. 8. Four different configurations for Si {311} and quartz $\{\bar{1}122\}$ series of experiments. In these cases θ_0, θ_G and φ_G are obtained as follows (cf. Text § 3):

Case I: $\theta_0=\pi/2-\varphi-\theta_B$, $\theta_G=\theta_0+2\theta_B$, $\varphi_G=\theta_G-(\boldsymbol{\nu}_e\boldsymbol{\nu}_a)$;
Case II: $\varphi_G=\pi/2-\varphi+\theta_B$, $\theta_G=\varphi_G+(\boldsymbol{\nu}_e\boldsymbol{\nu}_a)$, $\theta_0=\theta_G-2\theta_B$.
Case III: $\varphi_G=\pi/2-\varphi+\theta_B$, $\theta_G=\varphi_G-(\boldsymbol{\nu}_e\boldsymbol{\nu}_a)$, $\theta_0=\theta_G-2\theta_B$;
Case IV: $\theta_0=\pi/2-\varphi-\theta_B$, $\theta_G=\theta_0+2\theta_B$, $\varphi_G=\theta_G+(\boldsymbol{\nu}_e\boldsymbol{\nu}_a)$,

where θ_B is the Bragg angle, φ is the angle between the net plane and a surface and $(\boldsymbol{\nu}_e\boldsymbol{\nu}_a)$ is the wedge angle. In {311} series, $\varphi=58°\,31'$ and in quartz $\{\bar{1}122\}$ series $\varphi=42°\,16'$.

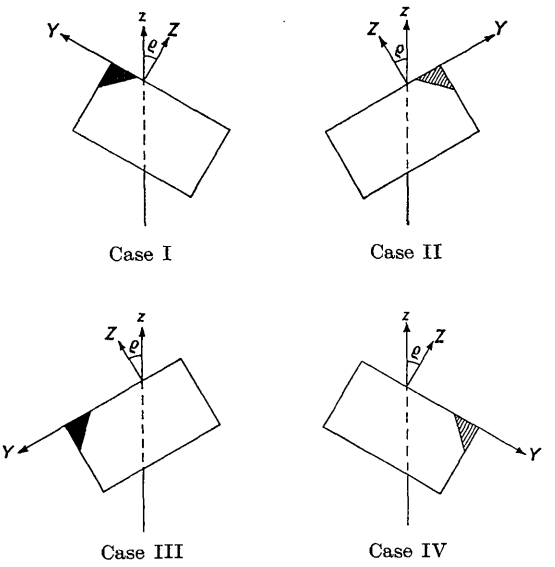

Fig. 9. Four different configurations for quartz R–r series. z is the direction of a vertical line and Y and Z are the Y- and Z-axis of quartz respectively. In these cases θ_0, θ_G and φ_G are determined as follows (cf. Text § 3):

Case I: $\theta_0=\theta_B$, $\theta_G=\theta_B$,
$\cos\varphi_G=\cos\theta_B\cos(\nu_e\nu_a)-\sin\theta_B\sin(\nu_e\nu_a)\sin\varrho$;

Case II: $\cos\theta_0=\cos\theta_B(1-\sin^2(\nu_e\nu_a)\sin^2\varrho)^{\frac{1}{2}}$
$+\sin\theta_B\sin(\nu_e\nu_a)\sin\varrho$,
$\cos\theta_G=\cos\theta_B(1-\sin^2(\nu_e\nu_a)\sin^2\varrho)^{\frac{1}{2}}$
$-\sin\theta_B\sin(\nu_e\nu_a)\sin\varrho$, $\cos\varphi_G=\cos\theta_B\cos\phi$;

Case III: $\theta_0=\theta_B$, $\theta_G=\theta_B$, $\cos\varphi_G=\cos\theta_B\cos(\nu_e\nu_a)$
$+\sin\theta_B\sin(\nu_e\nu_a)\sin\varrho$;

Case IV: $\cos\theta_0=\cos\theta_B(1-\sin^2(\nu_e\nu_a)\sin^2\varrho)^{\frac{1}{2}}$
$-\sin\theta_B\sin(\nu_e\nu_a)\sin\varrho$,
$\cos\theta_G=\cos\theta_B(1-\sin^2(\nu_e\nu_a)\sin^2\varrho)^{\frac{1}{2}}$
$+\sin\theta_B\sin(\nu_e\nu_a)\sin\varrho$, $\cos\varphi_G=\cos\theta_B\cos\phi$;

where θ_B is the Bragg angle and ϱ is the angle between z and Z, the angle ϕ is determined by $\tan\phi=\tan(\nu_e\nu_a)\cos\varrho$.

to the geometric conditions. Firstly we have to find the angles θ_0, θ_G and φ_G. In the following we deal with two experimental situations: (*a*) ν_e and ν_a are in the horizontal plane, in other words the edge of the wedge is vertical, but the net plane is oblique to both crystal surfaces; and (*b*) the edge is oblique to a vertical line but the net plane is perpendicular to one of the crystal surfaces, in other words ν_e or ν_a lies in the net plane. In our experiments the plane of the ribbon-shaped incident beam was always vertical and the mean direction of the beam was horizontal. The normal to the net plane was always kept in the horizontal plane.

In condition (*a*) we can obtain $\cos\theta_0$, etc., for four different cases which are illustrated in Fig. 8. The results are shown in the legend. In case (*b*) the configurations are a little complicated, but still we can obtain $\cos\theta_0$, etc., for the practically-used four cases as shown in Fig. 9, with the results summarized in the legend.

Next we have to consider the effect of vertical divergence of the incident beam. The X-ray source is placed at a finite distance from the specimen therefore the X-rays diverge vertically. We cannot put the recording film just behind the specimen because of the screen needed to cut off the direct beam. As a first approximation we consider that the observed pattern is a projection on to the film of the theoretical pattern located in the plane of the specimen. This assumption was verified by measuring the fringe separations in section patterns obtained with different specimen-to-film distances. Thus it is necessary to make a small but appreciable correction to the fringe-spacing values given by equation (3).

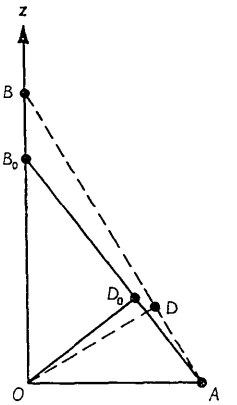

Fig. 10. Change of fringe distances due to vertical divergence of an incident beam.

In Fig. 10, z is the vertical axis, AB_0 is a fringe line of the ideal pattern and OA is a horizontal line. Since a vertical distance is elongated but a horizontal distance is not changed in the observed pattern, the corresponding observed fringe line should be the dotted line AB. Therefore the observed fringe separation $\delta=OD$ is $\delta=\delta_0\cos\sigma/\cos\sigma_0$ where $\delta_0=OD_0$ is the fringe separation in the ideal pattern corresponding to the observed δ, and σ and σ_0 are the angles between the z-axis and fringe lines in observed and ideal patterns, respectively. However,

$$OB_0\tan\sigma_0=OB\tan\sigma$$

and

$$OB=OB_0(D+L)/D$$

where D is the distance from X-ray source to specimen and L is the specimen-to-film distance.

Hence

$$\tan\sigma=\tan\sigma_0 D/(D+L)\,. \qquad (5)$$

As an example, if we put $D\simeq 30$ cm., $L\simeq 2{\cdot}5$ cm. and $\sigma=45°$ as reasonable figures, the correction amounts to between two and three per cent.

4. Comparison between theory and experiment

Equation (3) shows that fringe separations depend upon the wavelength λ and the geometrical factors $(\cos\theta_G/\cos\theta_0)^{\frac{1}{2}}$ and Φ. We performed three series of ex-

periments to check these points. The first two series were carried out to test the geometric factors, using Mo $K\alpha_1$ radiation, and the third was concerned with wavelength effects, using Mo $K\alpha_1$ and Ag $K\alpha_1$ radiation.

(i) *Silicon* {311} *series*

A wedge crystal of silicon was made from a {111} plate. Using this crystal we obtained traverse patterns for four different geometrical conditions of reflection, one such pattern being shown in Fig. 4. Details of the wedge and of the geometric configurations are given in the legends of Figs. 4 and 8. Experimental results and calculated values of fringe separations are listed in Table 1. The calculations are based upon a value

Table 1. *Silicon* {311} *series of experiments*

Case	Net plane	Fringe spacing Obs., mm.	Calc., mm.	Calc./Obs.
I	$(3\bar{1}1)$	0·107	0·114	1·06
II	$(\bar{1}31)$	0·059	0·061	1·03
III	$(\bar{3}1\bar{1})$	0·098	0·103	1·05
IV	$(1\bar{3}1)$	0·047	0·053	1·15

of the atomic scattering factor of silicon, 8·2, which was obtained by graphical interpolation from the data for neutral silicon (Peiser, Rooksby & Wilson, 1955). For the $\sin\theta/\lambda$ value of the 311 reflection, bonding-electron configuration has little effect on the f-value. Still, the above value might have an error of a few per cent. Moreover, there is the already-mentioned doubt concerning the parameter y. Therefore we should hardly expect complete agreement between calculated and experimental values. Their ratios, however, should coincide with each other because an X-ray reflection of the same index is used throughout this series of experiments. Actually the agreement is fairly good, except in Case IV. Here, however, fringe separations are very small and the fringes themselves are very faint so that this discrepancy may be attributed to experimental errors in measuring the fringe separations.

(ii) *Quartz* {11$\bar{2}$2} *series*

Similar experiments were carried out using a quartz crystal. A wedge was made from an X-cut plate. The wedge angle was 11° 16′ and the wedge axis was the Y-axis of the quartz. Four configurations of reflection were considered in a similar way to the silicon {311} series. In the present case, however, the reflections 11$\bar{2}$2 and $\bar{1}\bar{1}$22 have slightly different structure amplitudes. According to Wei (1935) they are 21·6 and 21·9 respectively. Still, changes of fringe spacing are almost all due to geometric effects, with a minor dependency upon net plane. The ratios of observed to calculated values should coincide for each group of experiments carried out for the same net plane. Moreover, if Wei's values of structure factor are correct, the ratios of the two groups should also agree with each other. As shown in Table 2, a nice agreement is obtained within each group, though a little systematic discrepancy is noticed.

Table 2. *Quartz* $\bar{1}\bar{1}22$ *series of experiments*

Case	Net plane	Fringe spacing Obs., mm.	Calc., mm.	Calc./Obs.
I	$\bar{1}\bar{1}22$	0·168	0·179	1·06
II	$11\bar{2}2$	0·099	0·103	1·04
III	$11\bar{2}\bar{2}$	0·151	0·166	1·10
IV	$\bar{1}\bar{1}2\bar{2}$	0·089	0·091	1·03

(iii) *Quartz R and r series*

We have obtained several traverse patterns using two different radiations, the wedge crystal being the same as that used in the {11$\bar{2}$2} series of experiments. Geometrical details are explained in the legend of Fig. 6, which shows a typical pattern of this series, and in Fig. 9. We have compared the R and r reflections using both Mo $K\alpha_1$ and Ag $K\alpha_1$.

For different radiations the geometrical factors change slightly as a consequence of the change in Bragg angle. This effect, however, is of the order of 3% or less. Consequently this series of experiments serves directly to check the wavelength effect. The results are shown in Table 3. In this case the ratios

Table 3. *Quartz R–r series of experiments*

(*a*) Wave length dependency.

		Fringe spacing, mm. Ag $K\alpha_1$	Mo $K\alpha_1$	Ratio Ag/Mo
R	obs.	0·291	0·231	1·26
	calc.	0·307	0·242	1·27
r	obs.	0·428	0·351	1·22
	calc.	0·503	0·394	1·28

of Ag-fringe separations to Mo-fringe separations should be independent of structure amplitude and should correspond with the corresponding calculated ratios. Moreover, since the R and r planes are both normal to the X-cut plate, and their Bragg angles are the same, their geometric factors are almost equal. Therefore the ratios for the R and r reflections should be equal. These points are well satisfied experimentally as shown in the last column of Table 3.

We have thus obtained a good agreement between experimental and theoretical dependence on wavelength and geometrical factors. We find, however, two systematic discrepancies between calculated and observed values. First, all observed values of fringe spacing are somewhat less than the values calculated by equation (3) assuming $y=0$. This suggests that we should take a slightly larger value for the parameter y. However, the section experiments and our preliminary interpretation of them show that such an attempt to improve the theory has no reliable basis.

Secondly, the ratio of calculated to observed value

is systematically larger for some net planes than for others. A possible explanation of this discrepancy is that the values of structure amplitude adopted above are not adequate. In particular, the quartz *R–r* series of experiments shows that this explanation is very plausible. In Table 4 we show the ratio of calculated

Table 4. *Quartz R–r series of experiments*

(*b*) The ratio of calculated fringe spacings to the observed values

Net plane	Mo $K\alpha_1$	Mo $K\alpha_1$	Ag $K\alpha_1$
r	$1{\cdot}12_2$ (I)	$1{\cdot}12_1$ (II)	$1{\cdot}17_5$ (I)
R	$1{\cdot}04_7$ (III)	$1{\cdot}03_4$ (IV)	$1{\cdot}05_4$ (III)

to experimental values of fringe separations for the *r* and *R* reflections, with Mo $K\alpha_1$ and Ag $K\alpha_1$ radiations, and with geometric configurations (indicated by Roman numerals) as explained in Fig. 9. The ratio for the *r*-reflection is systematically larger than that for the *R*-reflection. As the *R* and *r* reflections have the same Bragg angle, and moreover, the geometrical arrangement of the *r*(I) case is quite similar to that of the *R*(IV) case, and of the *R*(III) case to that of the *r*(II) case, therefore we can find no reasonable way to explain this discrepancy other than to assume a different value of the structure amplitude of the *r*-plane. Thus F_r should be larger than Wei's value at least by an amount necessary to decrease the ratio of calculated to observed values to 1·05, the average value of the ratio for the *R*-reflection. This amount is about 9%.

In the quartz $\{\bar{1}\bar{1}22\}$ series, the ratios in cases I and III are a little larger than in cases II and IV. This suggests that the structure amplitude of the $\bar{1}\bar{1}22$ reflection should be larger than Wei's value by about 4%.

We arrive thus at the conclusions, that the structure amplitude of reflections from the *r* and $(\bar{1}\bar{1}22)$ planes should be changed by several per cent, and that in spite of this, there remains a small systematic discrepancy between all experimental and calculated values of the order of four to five per cent. This latter point we consider in § 5.

5. Discussion

The fact that 'Pendellösung' fringes can be observed in the X-ray case is significant in three respects, which we can summarize as follows:

(*a*) It is probably the most direct demonstration possible that an actual crystal can be considered ideally perfect from the standpoint of X-ray diffraction. In other words, this kind of observation may be used to prove the perfectness of a crystal. For example, we found a few 'Pendellösung' fringes along grain boundaries as shown in Fig. 5. This shows that elastic distortion of the lattice around grain boundaries is confined within a very thin region, as expected from dislocation theory (Kato & Lang, in preparation). In another example, as described in § 2 (iii), we could infer the existence of a new type of plane defect in quartz crystals through an observation of 'Pendellösung'. Here the plane defect is detected by the loss of phase relationship it causes.

(*b*) From the standpoint of X-ray diffraction phenomena, study of 'Pendellösung' fringes is important for testing how extensively the dynamical theory can be applied to an actual crystal under practical experimental conditions. The fair agreement between theory and experiment as described in § 3 shows that the ordinary dynamical theory is satisfactory in essential points.

(*c*) The measurement of fringe spacings gives us the possibility of determining precisely the structure amplitude of low-order reflections. The usual method for such a determination, the measurement of intensity of reflection, has always some uncertainty because the intensities of low-order reflections depend to such a large extent upon the perfectness of the crystal, and we have no reliable theory for predicting the intensity expected from real crystals. Some methods have been proposed which have a more reliable basis, such as the asymmetric reflection method (Gay, 1952) and the polarized X-rays method (Ramasechan & Ramachandran, 1953). These procedures have some advantages but their accuracy seems to be about ±10%, and intensity measurements must still be used.

On the other hand, the method described in this paper enables us to estimate structure amplitudes from measurement of fringe separations and a wedge angle, without using any intensity measurement. As pointed out in § 4, at the present stage there seems to be a small systematic discrepancy of 4 to 5% in obtaining an absolute value of the structure amplitude. If this discrepancy can be removed we might be able to obtain structure amplitudes with an accuracy of ±1% in favorable cases such as the quartz *R* and *r* reflections, as shown in Table 4.

As yet we cannot explain this discrepancy. An allowance for thermal vibration would not reduce it. Anomalous dispersion acts in the right way to reduce it, but it is a very small effect, and the discrepancy, moreover, is the same for both Ag and Mo radiations. Actually, we must regard the present theory as temporary, as will be pointed out below.

In the section experiments we obtained very interesting patterns due to both the diffracted beam and the primary beam, as shown in Fig. 7. The intensity distributions of these patterns are complementary to each other: a white line in the one corresponding to a black line in the other, and vice versa. This may easily be understood if we consider the energy exchange between primary and diffracted beams. It seems worthwhile to notice here that the usual electron microscope image (bright field image) corresponds to the primary-beam pattern, and the dark field image corresponds to the diffraction pattern. With electrons we can observe 'Pendellösung' fringes in both cases.

In the electron case section patterns cannot be obtained. In the X-ray case, section patterns are quite fundamental because traverse patterns are just superimposed section patterns. Thus it is very desirable to gain a satisfactory understanding of section patterns.

The section patterns cannot be explained by the dynamical theory described in the prevailing textbooks (for example Zachariasen, 1945; James, 1954), because this concerns the intensity of a plane wave which is associated with a wave vector or the intensity distributions in a region which is less than the width of the wave front of a plane wave as in Laue's explanation of Kossel patterns (Laue, 1935).

In section patterns we have to consider the intensity distributions in a region much larger than an incident beam size. For this reason we have to consider the energy flow in a crystal. According to the recently developed theories (Kato, 1952, 1958(*b*); v. Laue, 1952, 1953; Ewald, 1958), if reflected waves occur, the energy flows in the direction of the normal to the dispersion surface characteristic of the reflection. Thus we expect that the X-rays go through the crystal in two different directions corresponding to the two branches of the dispersion surface. These directions are determined by the direction of the incident plane wave (the parameter y) and always lie between the direction of the direct beam and of the reflected beam expected by the Bragg relation. In our actual experiments, however, the X-ray energy goes through the crystal within the whole range of directions between the two above-mentioned ones, because the incident beam is not strictly collimated and so its angular divergence covers the whole angular range in which the incident beam is reflected appreciably. Thus we expect section patterns to have a definite width appropriate to the crystal shape and Bragg angle as shown in Fig. 2. A more detailed treatment of this point will be given in another paper (Kato, in preparation).

The theory which was developed for electrons (equation (3)) assumes that interference occurs between two beams which are excited by one incident plane wave specified by a parameter y. This is permissible in the case of electrons because the wave fronts of the two beams are large enough to overlap.

With X-rays these conditions are not satisfied. Actually section patterns show that interference is occurring between two beams which propagate in the same direction in the crystal, and which are two elements of a spherical wave front corresponding to parameters y and $-y$. Thus the theory developed for electrons seems inadequate for the interpretation of section patterns. Hence the small discrepancy between the theory and experiments, as detailed in § 4, can not be removed by simply giving y in (3) a non-zero value.

The above considerations lead us to the important conclusion that either the boundary conditions or the assumption of a plane wave as incident in the usual dynamical theory have to be modified because otherwise we cannot obtain in the general case interference between two waves propagating in the same direction in the crystal. While further discussion of this point will be postponed, it seems worthwhile to point out that the usual theory should give us a nearly correct result as long as we are concerned with the interference fringes due to the two beams which propagate in the direction corresponding to $y=0$. It is also expected that the amplitude of the interference pattern in a section experiment is a maximum along a line corresponding to this direction. The authors believe that this is the reason why the above theory could predict the fringe separations quite well.

This work was made possible by a grant from the National Science Foundation which is gratefully acknowledged. We would like to thank Dr J. R. Patel for providing us with Si single crystals. We also wish to thank Prof. P. P. Ewald for his interest and helpful discussion.

References

Cowley, J. M. & Rees, L. G. (1946). *Nature, Lond.* **158**, 550.

Cowley, J. M. & Rees, L. G. (1947). *Proc. Phys. Soc., Lond.* **59**, 283.

Ewald, P. P. (1916). *Ann. d. Phys. (Lpz.)*, **49**, 117; see also (1933). *Handbuch der Physik*, **23**, 2; 290. Berlin: Springer.

Ewald, P. P. (1958). *Acta Cryst.* **11**, 888.

Gay, P. (1952). *Acta Cryst.* **5**, 525.

Hall, C. E. (1948). *J. Appl. Phys.* **19**, 198.

Heidenreich, R. D. (1942). *Phys. Rev.* **62**, 291.

Honjo, G. (1953). *J. Phys. Soc., Japan*, **8**, 776.

Honjo, G. & Mihama, K. (1954). *J. Phys. Soc., Japan*, **9**, 184.

James, R. W. (1954). *The optical principles of the diffraction of X-rays*. London: Bell.

Kato, N. (1949). *Proc. Jap. Acad. Soc.* **25**, 41.

Kato, N. (1952). *J. Phys. Soc., Japan*, **7**, 397.

Kato, N. (1953). *J. Phys. Soc., Japan*, **8**, 350.

Kato, N. (1957). *Acta Met.* **5**, 237.

Kato, N. (1958*a*). *Acta Met.* **6**, 647.

Kato, N. (1958*b*). *Acta Cryst.* **11**, 885.

Kato, N. In preparation.

Kato, N. & Lang, A. R. In preparation.

Kinder, E. (1943). *Naturwiss.* **31**, 149.

Kossel, W. (1943). *Naturwiss.* **31**, 323.

Lang, A. R. (1958). *J. Appl. Phys.* **29**, 597.

Lang, A. R. (1959). *Acta Cryst.* **12**, 249.

Laue, M. v. (1935). *Ann. d. Phys. (Lpz.)*, **23**, 705.

Laue, M. v. (1940). *Naturwiss.* **28**, 645.

Laue, M. v. (1952). *Acta Cryst.* **5**, 619.

Laue, M. v. (1953). *Acta Cryst.* **6**, 217.

Niehrs, H. (1954). *Z. Phys.* **138**, 570.

Peiser, H. S., Rooksby, H. P. & Wilson, A. J. C. (Editors). (1955). *X-ray Diffraction by polycrystalline Materials*. London: Institute of Physics. Appendix Table 9, p. 656.

RAMASECHAN, S. & RAMACHANDRAN, G. N. (1953). *Acta Cryst.* **6**, 364.
STURKEY, L. S. (1948). *Phys. Rev.* **73**, 183.
WEI, P. (1935). *Z. Kristallogr.* **92**, 355.
ZACHARIASEN, W. H. (1945). *Theory of X-ray Diffraction in Crystals*. New York: Wiley.

Acta Cryst. (1959). **12**, 794

The Treatment of Errors in the Isomorphous Replacement Method

BY D. M. BLOW AND F. H. C. CRICK

Medical Research Council Unit for Molecular Biology, Cavendish Laboratory, Cambridge, England

(*Received* 28 *July* 1958 *and in revised form* 5 *November* 1958)

This treatment is intended for complex structures where conventional refinement is impossible. A method is described for assessing the errors which arise in applying the isomorphous replacement method. Both errors due to non-isomorphism and observational errors are considered. Probability functions are derived which give, in the centrosymmetric case, the probability of a correct sign determination, and in the non-centrosymmetric case the relative probabilities of different phases. These probabilities may be used to calculate a 'best' Fourier, in which the errors in electron density are minimized, and also to estimate the r.m.s. error in this 'best' Fourier.

There are two steps in the application of the isomorphous replacement method. The first is the determination of the position of the outstanding features (usually a small number of heavy atoms) which differentiate a pair of isomorphous structures. The contribution $\mathbf{f}_c$ of this part of the structure to the structure factors may then be calculated. The second step is the use of these calculated contributions to determine the phases of the reflexions. This is done by comparing them with the observed intensity differences. In this way the structure may be determined.

This paper is concerned with the second step. There will be many reflexions for which $\mathbf{f}_c$ is very small. The determination of phase will be correspondingly poor. How should these reflexions be treated? In non-centrosymmetric structures, as is well known, unambiguous phase determinations are possible only if at least three isomorphous compounds are available. How should the results from the two pairs be combined? With simple structures where atoms are resolved, a trial structure can be obtained, and refinement made, for instance by the least-squares method. With a large protein, there is no immediate prospect of resolving the individual atoms and therefore no way of refinement from a trial structure. The accuracy of the final Fourier is dependent on the best choice of weights and phases during the second step of the calculation. There will be cases of intermediate complexity where the right trial structure will be found only if the second step is done accurately enough.

We will describe a method for treating this question as rigorously as possible. A structural study where the method has been put to practical use has been published elsewhere (Blow, 1958).

Estimation of error

The errors with which we are concerned are those which arise in the use of the isomorphous replacement method. It will be assumed that the 'true' structure would be the Fourier transform of accurately observed structure factors, given the proper phases. Errors which arise due to series termination and extinction are not considered.

Let $\mathbf{F}$, $\mathbf{F}_H$ be the structure factors of two isomorphous compounds, the latter containing additional heavy atoms. We will define

$$\mathbf{f}_H = \mathbf{F}_H - \mathbf{F} \,. \tag{1}$$

The basis of the isomorphous replacement method is to calculate an approximation to $\mathbf{f}_H$, which we will call $\mathbf{f}_c$, usually by assuming the differences are entirely due to heavy atoms whose coordinates have been determined. (1) then gives information about the phases.

Centrosymmetric case

If the structures are centrosymmetric, then $\mathbf{F}$, $\mathbf{F}_H$, $\mathbf{f}_H$, $\mathbf{f}_c$ are all real. Either

$$|\mathbf{f}_H| = |\mathbf{F}_H - \mathbf{F}| \tag{2a}$$

or

$$|\mathbf{f}_H| = |\mathbf{F}_H + \mathbf{F}| \tag{2b}$$

the latter case arising only when the signs of $\mathbf{F}_H$ and $\mathbf{F}$ are different. If we exclude all cases where $\mathbf{F}_H + \mathbf{F} < \mathbf{f}_c(000)$, the maximum possible value of $\mathbf{f}_c$, we can approach certainty that (2*a*) applies. In these cases, a direct assessment of error may be made.